Interference fringe-free transmission spectroscopy of amorphous thin films

Tong Li, Jerzy Kanicki,[a] Wei Kong, and Fred L. Terry, Jr.
Department of Electrical Engineering and Computer Science, Solid State Electronics Laboratories, The University of Michigan, 1246-D EECS Building, 1301 Beal Avenue, Ann Arbor, Michigan 48109

(Received 21 January 2000; accepted for publication 10 July 2000)

Based on optical fundamentals, we present in this article a practical method to obtain an interference fringe-free transmission spectrum for hydrogenated amorphous solid thin films. From this spectrum, reliable optical properties, such as the Urbach edge and optical band gap of the thin films, can be extrapolated directly. In terms of the Brewster angle accuracy, the margins of error of the proposed method due to material dispersion are less than $\pm 1\%$ for hydrogenated amorphous silicon and less than $\pm 1.2\%$ for hydrogenated amorphous silicon nitride. These figures are less than the detectable limit of the proposed method. © *2000 American Institute of Physics.* [S0021-8979(00)02720-1]

I. INTRODUCTION

Hydrogenated amorphous silicon (a-Si:H) and silicon nitride (a-SiN$_x$:H) are the materials used in amorphous silicon thin-film transistor (a-Si:H TFT) structures. Their optical properties such as position and shape of the absorption edge, are of particular interest to a-Si:H based optoelectronic devices.[1] Various methods have been used to measure the absorption constant (α) of these thin solid films. Among those, the most popular methods in the range of $\alpha < 10^3$ cm^{-1} are primary and secondary photoconductivity,[2,3] photoacoustic spectroscopy,[4] photothermal deflection spectroscopy;[5] and for higher α values, ultraviolet optical transmission spectroscopy is often used.[6] In general, the measured characteristics by these methods are hard to analyze accurately without removal of the interference fringes caused by multireflection interference of thin films. These interference fringes significantly distort the optical spectra at lower α values. The removal of the interference fringes is normally accomplished by subtracting them from the measured optical spectrum. These subtracting patterns are mathematically generated fringes that best match fringes embedded in the measured characteristic.[7] This type of fringe-matching and subtracting method is tedious and inconvenient in practice. More importantly, it can hardly remove the fringes to a satisfactory level, since the generated pattern can never match perfectly with the embedded pattern.

This article describes a method based on some fundamental optical principles to obtain an optical density spectrum free of interference fringes. And to show clearly the potential of this method, the significant discrepancies between optical properties derived from fringe-free and fringe-distorted optical spectra are illustrated. Furthermore, the spectrum dependence on the light incident condition is analyzed. Application of the proposed method to solid thin film characterization is also presented. Finally, based on examples shown in this article, the critical issues and steps of this method are discussed.

[a]Author to whom correspndence should be addressed; electronic mail: kanicki@eecs.umich.edu

II. EXPERIMENTAL

The a-Si:H and a-SiN$_x$:H thin films were deposited on glass and quartz substrates in a plasma-enhanced chemical-vapor-deposition (PECVD) system, respectively. The substrate temperature was set at 250 °C, and the chamber pressure was kept at 0.43 Torr during the process. Gas flow rates were (silane) 50 standard cubic centimeter per minute (sccm) for a-Si:H, and (silane) 18 sccm and (ammonia) 200 sccm for a-SiN$_x$:H. The films' thickness and refractive indices were then measured using the Dektak surface profiler and Sopra GESP-5 spectroscopic ellipsometer/photometer system.

Rotating polarizer ellipsometric measurements were performed in the tracking analyzer mode, at an incident angle of 75°. In the spectroscopic ellipsometry experiment, the complex ratio of Fresnel reflection coefficients is measured as a function of wavelength, which is given by

$$\rho = \frac{r_p}{r_s} = \tan\Psi \exp(i\Delta), \tag{1}$$

where r_p and r_s are the complex Fresnel reflection coefficients for light polarized parallel and perpendicular to the plane of the light incidence, respectively, and ψ and Δ are the ellipsometry angles. In our experiment, tan(ψ) and cos (Δ) are the quantities measured directly.

To parametrize the dielectric functions of amorphous silicon, Forouhi and Bloomer's model was used.[8] The parameters and the thickness of the thin film were determined by the Levenberg–Marquard regression method, in which the ellipsometry parameters tan(ı) and cos(Δ) were calculated from trial values of the parameters and thickness. This calculation was carried out while it iterated on the unknown parameters until a desired deviation between the measured and calculated spectra was obtained.

The films' optical density was measured at room temperature using a Varian Cary 5E UV–Vis–NIR spectrophotometer. For the sample settings, a pair of Harrick Glan Taylor linear polarizers were used to produce p-polarized probe beams, and Brewster's angle sample holders were used to adjust the beam's incident angle. For the instrument settings,

 © 2000 American Institute of Physics

two exchangeable light sources and a single detector were used in the measurement. These two lamps cover ultraviolet and visible ranges, respectively, and they switch from one region to another at a wavelength of 310 nm. The instrument's scan rate was set at 1800 nm/min and a double-beam model was used in the scanning. The scanning itself has a spectral resolution and bandwidth of 1 and 2 nm, respectively. Finally, a unity energy level and full slit height were adopted in the measurement.

III. THEORETICAL FUNDAMENTALS

A. Optical properties of amorphous solid thin films

In amorphous materials there are generally three different absorption regions which can be modeled mathematically by different functions. At large absorption (α), the absorption is attributed to the extended states, and is normally defined by the Tauc equation[9]

$$\sqrt{\alpha \times E_{\text{photon}}} = B(E_{\text{photon}} - E_{\text{Tauc}}), \tag{2}$$

where B is the slope at the large α (linear region), and E_{photon} and E_{Tauc} are the photon energy and Tauc optical band gap in eV, respectively. The Tauc optical band gap is obtained from the $\sqrt{\alpha \times E_{\text{photon}}}$ vs E_{photon} plot by a linear extrapolation.

At a small a value of α (typically, less than 10^3 and 10^4 cm^{-1} for a-Si:H and a-SiN$_x$:H, respectively), the dependence of α on photon energy appears to be exponential:[8]

$$\alpha \approx \exp\left(\frac{E_{\text{photon}}}{E_0}\right) \tag{3}$$

where E_0 is the so-called Urbach energy (edge), which is related to the slope of the valence band tail and can be extrapolated from the semilogarithm plot of α vs E_{photon}. In addition, the material optical band gap defined at $\alpha = 10^4$ cm^{-1} (E^{04}) is also commonly determined from this plot.

At low photon energy (for $\alpha < 10^2$), the curve of the semilog plot flattens out, and the α is attributed to the point defect (deep gap states) absorption. This absorption is mainly affected by the film's doping level and preparation process, and is normally detected by other means such as photoacoustic and photothermal deflection spectroscopic techniques.[2,4,5]

Since the film's optical properties defined by Eqs. (2) and (3) are extracted from the film's transmission spectrum, the accuracy of this spectrum is crucial in determining these important material's properties. Generally, the film's transmission spectrum measured for the film set at normal to the probe beam contains interference fringes. The fringe effect on the absorption spectrum is normally insignificant in the large absorption range, since in this region most of the energy of the light is absorbed and very little left to form an interference pattern. In contrast, in the small absorption range, the fringe effect is very serious since most of the energy of the light is engaged in the interference. Hence, the fringe distortion appears to be much worse at low photon energy (small absorption) in comparison with that at the high photon energy (large absorption). This fringe effect is exaggerated in the semilog plot in which the relative values are emphasized. Therefore, the removal of the interference fringes has a great impact on the absorption coefficient plot, especially at the edge of the absorption band tail.

B. Thin-film optics

It is well known that when a beam of the light passes through a thin film with the thickness comparable to the light wavelength, a pattern of the interference fringes can be generated due to constructive and destructive interference of the reflected and transmitted light components from various interfaces.[10,11] Since an unpolarized light beam can be viewed as a sum of a p- (electrical field vibrating within the plane parallel to the light incident plane) and s-polarized light (electrical field vibrating perpendicular to light incident plane), these interference fringes are, in fact, the superimposition of the fringes caused by p- and s-polarized light beams. The amplitude and period of these fringes are determined by the interfacial reflectances and optical path within the film, respectively. The reflectance of p- and s-polarized light (R_p and R_s) strongly depend on the beam's incident angle and the film's refractive index, and can be given by[10]

$$R_p = \frac{\tan^2(\theta_i - \theta_r)}{\tan^2(\theta_i + \theta_r)}, \tag{4.1}$$

$$R_s = \frac{\sin^2(\theta_i - \theta_r)}{\sin^2(\theta_i + \theta_r)}, \tag{4.2}$$

where θ_i and θ_r are light incident and refracted angles, respectively.

It is clear that if the denominator of the Eq. (4.1) is infinite, the reflectance of p-polarized light vanishes. The light incident angle that satisfies this condition is called the Brewster angle, and can be expressed by[10]

$$\tan \theta_B = \frac{n_r}{n_i}, \tag{5}$$

where n_{r} and n_{i} are refractive indices of the refracting and incident media, respectively.

The variations of R_p and R_s with the light incident angle for a-SiN$_x$:H and a-Si:H are plotted in Fig. 1. These curves were calculated using $n_{a\text{-SiN}_x\text{:H}} = 1.96$ (measured at $\lambda = 360$ nm) and $n_{a\text{-Si:H}} = 4.01$ (measured at $\lambda = 700$ nm) according to Eq. (4). From Fig. 1 the Brewster angles of 63° for a-SiN$_x$:H and 76° for a-Si:H can be deduced. At the Brewster angle, p-polarized light fully transmits into the second medium without any reflection, thus, no interference fringe can be observed.

C. Material dispersion

It should be clear that the Brewster condition is, by definition, only valid in the spectral region in which the refractive index does not change with the photon energy apprehensibly. For a wide band spectrum with a significant index variation, the Brewster angles should be determined for indices corresponding to certain spectral regions. In the current study, the spectral region that is greatly impacted by the interference fringes is located at the low absorption edge, while the large absorption spectral region is not affected by

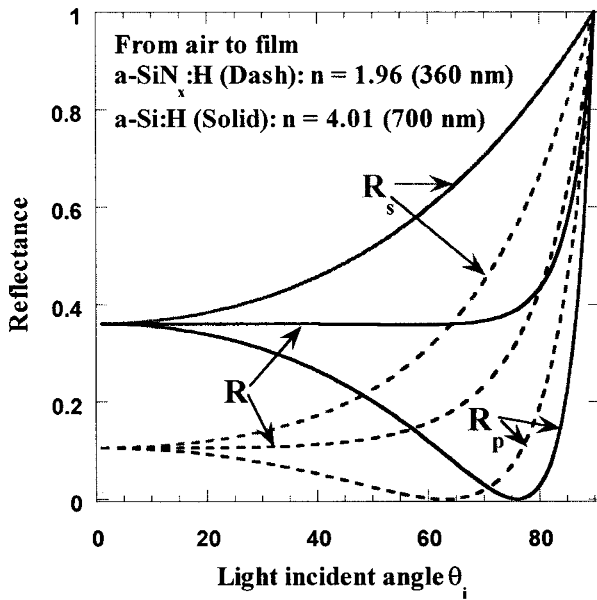

FIG. 1. Interfacial reflectances as functions of the external light incident angle for *a*-Si:H and *a*-SiN$_x$:H, respectively. R, R_s, and R_p stand for average, *s*- and *p*-polarized components, respectively. The refractive indices used in the calculation are 4.01 and 1.96 for *a*-Si:H and *a*-SiN$_x$:H, respectively.

the fringe patterns. This greatly narrows the spectral region in which a common refractive index can normally be used.

As illustrated in Figs. 2(a) and 2(b) for *a*-Si:H and *a*-SiN$_x$:H, respectively, the refractive index (n) and extinction coefficient (k) vary with the photon energy. For *a*-Si:H, n increases with the photon energy until it reaches a maximum at around 2.9 eV, and then starts to decrease at higher photon energy; while k shows a monotone increase with the photon energy. For *a*-SiN$_x$:H, both n and k show a monotone increase with the photon energy. These n values agree well with those previously reported in the open literature.[12,13]

Overall, the dispersions observed for both films do not appear significant enough to affect the reliability of the proposed measuring method. It will be clear in subsequent sections that the spectral regions of the band tails of the *a*-Si:H and *a*-SiN$_x$:H are roughly within 1.6–2 and 3–4.7 eV, respectively, as indicated by the boxes in Fig. 2.[14] According to the measured data in Fig. 2, those regions correspond to the n variations of 3.82–4.24 for *a*Si:H and 1.93–2.07 for *a*-SiN$_x$:H. Meanwhile, the variations of the k values are so insignificant within these regions that they can be ignored. In other words, the variations of the calculated Brewster angle is less than $\pm 1\%$ for *a*-Si:H ($76.06° \pm 0.7°$) and within $\pm 1.2\%$ for *a*SiN$_x$:H ($63.4° \pm 0.8°$). These variations are insignificant to cause any apprehensible interfacial reflectance changes (see Fig. 1). Furthermore, these variations are much less than the resolution of the light incident angle setting, and will, of course, not affect the reliability of the proposed method.

It should be stressed that when the absorption of the thin film is nontrivial, the calculation of the interfacial reflectance is difficult, since the refractive index becomes complex due to the nontrivial presence of the extinction coefficient.[15,16] In current study, the extinction coefficients for both films are

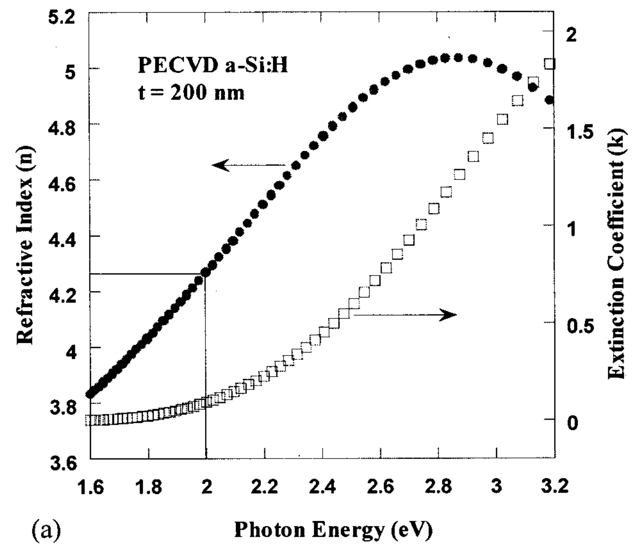

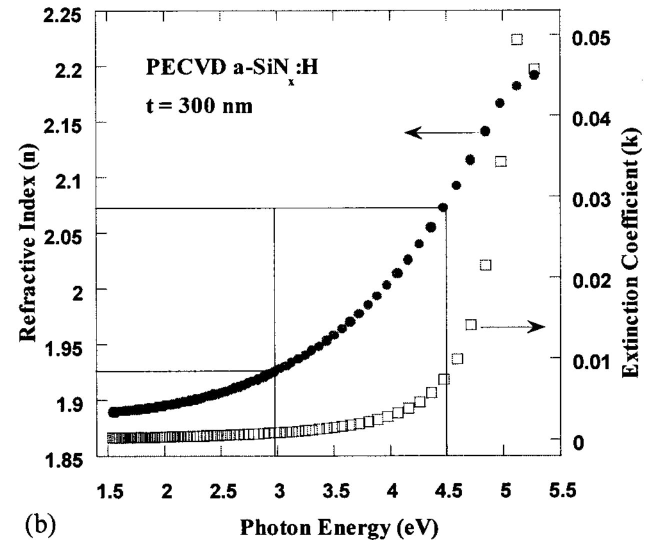

FIG. 2. Measured refractive indices and extinction coefficients of *a*-Si:H films (a) and *a*-SiN$_x$:H (b), respectively.

negligible, and moreover, their variations with the photon energy within the regions of interest are insignificant (within 0 to 0.01). Therefore, it is legitimate in this case to use only the real part of the refractive index as an effective refractive index in our calculations. This effective index can be calculated for a given light incident angle by using Eq. (5).

IV. OPERATION

The experimental setup (top view) used in this study is shown schematically in Fig. 3. An unpolarized beam from the light source is split into sample and background beams by a beam splitter. Both sample and background beams then impinge on linear polarizers set with their axis within the plane of the paper and orthogonal to the probe beam, as indicated by the line with double arrows. The thin-film sample is set at the position where the angle between its normal and probe beam is equal to θ_B. Then the transmissive spectrum is collected and normalized *in situ* by the detector at the left side. The sample and background should be

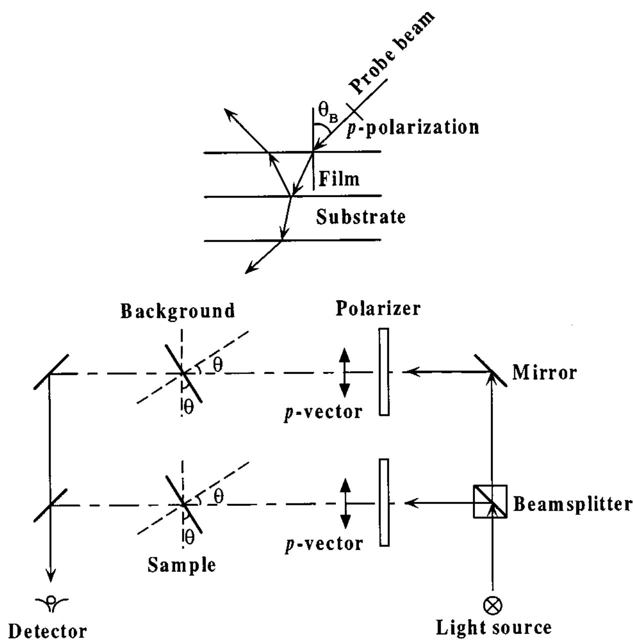

FIG. 3. Experimental setup used for interference fringe-free measurements.

set at the same angle, since different incident angles will result in different substrate effective thicknesses.

Theoretically, there are two possible Brewster conditions corresponding to the first and second film interfaces. When the Brewster condition of the first interface is satisfied, for *p*-polarized light, the interference fringes can be avoided, since the ultimate transmitted light reaching the detector contains no reflected component. This situation can be schematically described in the inset of Fig. 3. A *p*-polarized light beam strikes the first interface (from air to film) and fully transmits into the film. Part of this transmitted light beam is then reflected by the second interface (film and substrate). This reflected light beam fully transmits at the first interface again (from the film) into the air, and no partial reflection exists at this direction. Since the Brewster angle in the air and the resulting refracted angle in the film are complementary ($\theta_B+\theta_r=90°$),[9] the reflected angle within the film is also at the Brewster condition.[17] It might be argued that if the Brewster condition of the second interface (from the film to substrate) is satisfied, the fringe-free spectrum might also be achieved. However, the analysis showed that the second Brewster condition can hardly be met because the incident light angle with respect to the second interface is normally not large enough to reach the Brewster condition.[18] Furthermore, to achieve the Brewster condition of the second interface, a very large external light incident angle is required (larger than θ_B of the first interface), at which most of light energy will be lost due to high reflection by the first interface (see the reflectance curve of *p*-polarized light in Fig. 1 beyond θ_B). Therefore, the first Brewster angle is the only option in practice and the reflectance curves of the first interface shown in Fig. 1 are the only reference needed for the experimental setup.

It should be noted that so far only the reflection within the thin film was addressed and no reflection within the substrate was even mentioned. Since the thickness of the sub-

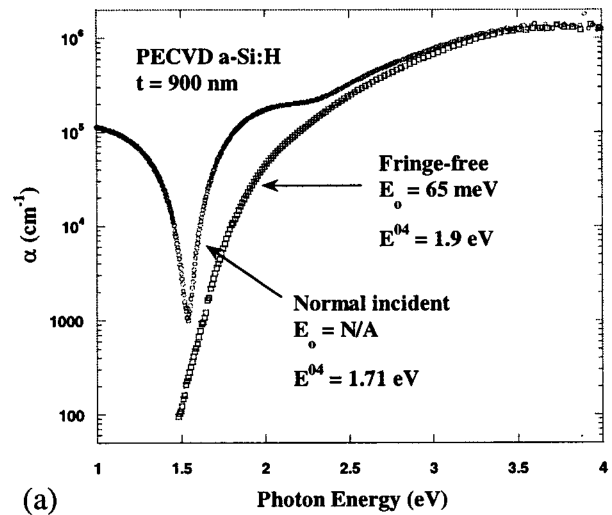

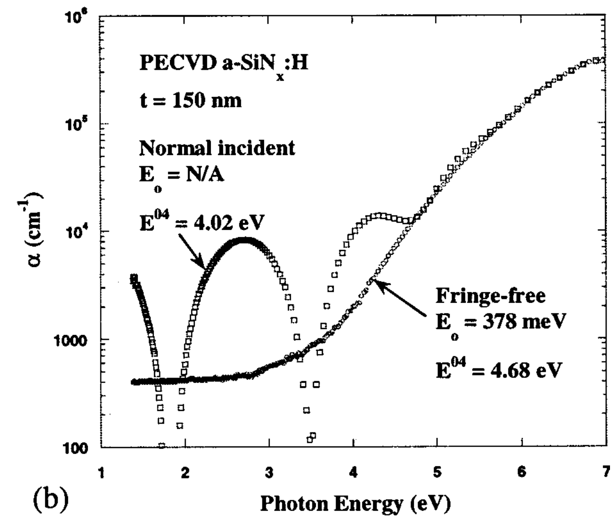

FIG. 4. Comparison of the absorption coefficients (α) measured at normal incidence and Brewster angle incidence with *p*-polarized light for (a) *a*-Si:H and (b) a-SiN$_x$:H. The Brewster incident angles are 76° and 63° for *a*-Si:H and a-SiN$_x$:H, respectively.

strate is usually very large compared to that of the film, it is, in fact, out of the spatial coherent range. The reflection within the substrate is incoherent and will not cause interference fringes in the spectrum. Therefore, the fringe analysis was always made with the assumption that the thickness of the substrate is infinite, and this assumption fits well with the experimental results.

V. EXPERIMENTAL RESULTS

A. Comparison between fringe-distorted and fringe-free spectra

The interference fringe-distorted and interference fringe-free absorption coefficients derived from the optical density measurements as a function of the photon energies are plotted in Figs. 4(a) and 4(b) for *a*-Si:H and a-SiN$_x$:H, respectively. The fringe-distorted spectra were measured with the film set at normal to the incident light, while the fringe-free spectra were taken with the light incident angles equal to 76° and 63° for *a*-Si:H and a-SiN$_x$:H, respectively. As in-

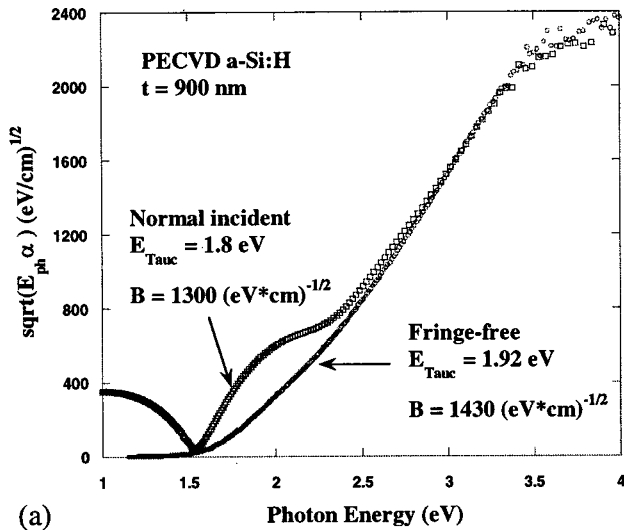

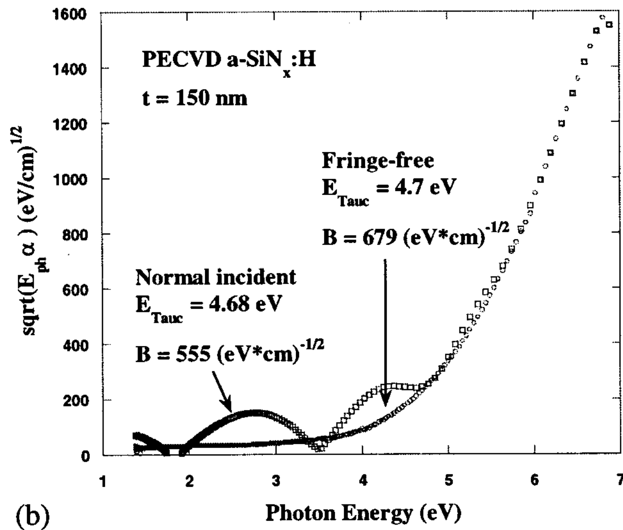

FIG. 5. Comparison of the $\sqrt{E_{\mathrm{photon}}\times\alpha}$ taken at normal incidence and Brewster angle incidence with *p*-polarized light for (a) *a*-Si:H and (b) *a*-SiN$_x$:H. The Brewster incident angles are 76° and 63° for *a*-Si:H and *a*-SiN$_x$:H, respectively.

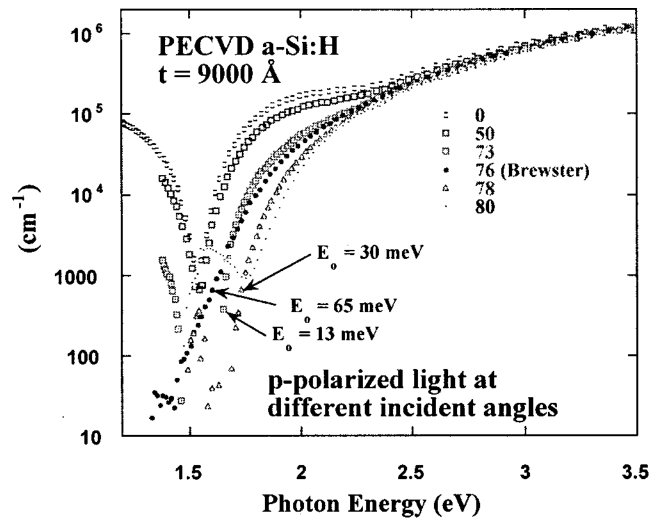

FIG. 6. Illustration of the influence of the light incident angle on the absorption coefficient vs photon energy spectra for the *a*-Si:H film.

dicated in Fig. 4, the difference between the fringe-distorted and fringe-free spectra is significant, especially at the low photon energies. For *a*-Si:H, the fringe-distorted spectrum gives an optical photon energy determined at $\alpha=10^4$ cm^{-1} (E^{04}) of 1.71 eV, while the extraction of the Urbach edge is impossible. On the other hand, the fringe-free spectrum clearly shows an E^{04} value of 1.9 eV and E_0 value of 65 meV. Similarly, for *a*-SiN$_x$:H, the fringe-distorted spectrum exhibits an E^{04} of 4.02 eV and no applicable Urbach edge. Meanwhile the fringe-free spectrum yields an E^{04} value of 4.68 eV and E_0 value of 378 meV.

The same spectra can be plotted again in the form of $\sqrt{\alpha\times E_{\mathrm{ph}}}$ versus the photon energy (E_{ph}), as shown in Figs. 5(a) and 5(b), whereas the fringe-distorted and fringe-free spectra are compared for *a*-Si:H and *a*-SiN$_x$:H, respectively. Although the differences between fringe-free and fringe-distorted spectra are not as significant as those are in Figs. 4(a) and 4(b), the deviations are still significant enough to be misleading. For example, for *a*-Si:H, the E_{Tauc} (extrapolated for $\sqrt{\alpha\times E_{\mathrm{ph}}}=0$) and B (slope) values derived from the fringe-free characteristics are 1.92 eV and 1430 (eV×cm)$^{-1/2}$, respectively; however, the same kind of values derived from the fringe-distorted spectrum are 1.8 eV and 1300 (eV×cm)$^{-1/2}$, respectively. Likewise, for *a*-SiN$_x$:H, E_{Tauc} and B values are 4.70 eV and 679 (eV×cm)$^{-1/2}$ for fringe-free spectrum, respectively, and the same kind of values are 4.68 eV and 555 (eV×cm)$^{-1/2}$ for fringe-distorted spectrum, respectively.

B. Light incident angle optimization

The impact of the light incident angle variation on the optical transmission spectrum is illustrated in Fig. 6 for *a*-Si:H. It is shown that the determination of a right Brewster angle is not an easy task. Without a careful analysis, spectra collected at 73°, 76°, and 78° in Fig. 6 could be regarded as fringe-free spectra, since no evident fringe patterns can be observed from the curves' shoulder edges. In addition, the subtle fringe patterns observed at the very low α are not always distinguishable from the noise. Apparently, quite different optical properties can be obtained from these spectra. For instance, spectra collected at 73°, 76°, and 78° yield E^{04} of 1.87, 1.90, and 1.99 eV, respectively; and Urbach edges of 13, 65, and 30 meV, respectively. Thus, it is important to set a convenient criterion for a correct light incident angle selection in order to maintain a certain level of consistency. Consequently, it is necessary to examine the impact of the variation of the light incident angle on the spectrum, and then draw a legitimate conclusion.

As shown in Fig. 6, the fringe impact is obvious at small incident angles such as at 0° and 50°, and this effect is significantly reduced when the incident angle approaches 73°. The edges of the spectra shoulders at the light incident angles of 73°, 76°, 78°, and 80° all appear to be smooth, which is one indication that the fringe impact is somewhat minimized. However, these shoulder edges are quite separated, which will result in not only different E^{04} values but also significantly different Urbach edge slopes. On the other

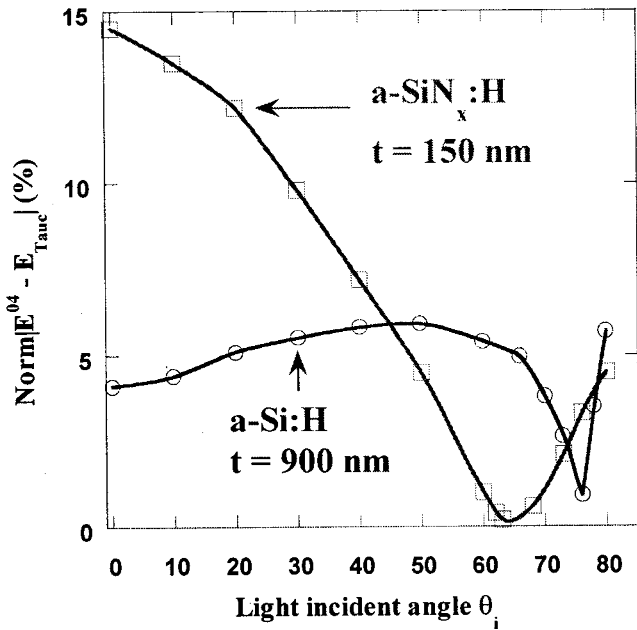

FIG. 7. Dependence of difference between E^{04} and E_{Tauc} on the light incident angle for a-Si:H and a-SiN$_x$:H, respectively. The difference is normalized by the optical E^{04} values obtained for each film. They are 1.90 and 4.68 eV, respectively, for a-Si:H and a-SiN$_x$:H films.

hand, it is observed that the patterns of the very edges of these spectra at low photon energies are relatively sensitive to the light incident angles. For the spectrum of 73°, this edge is obviously a fringe pattern. For the spectrum at 76°, the fringe pattern can hardly be recognized (less than 100 cm^{-1}), which appears to be merely the noise due to the detection limit of the instrument. For the spectrum at 78°, this edge, again, appears to represent a pattern but with an opposite phase to those collected at light incident angles of less than 76°. This trend becomes clearer in the spectrum collected at 80°, since the magnitude of this pattern is increased. It is clear from Fig. 6 that the spectrum collected at 76° represents the one (turning point) that separates the spectra with the opposite phases. Therefore, it could be concluded that the solid dots in Fig. 6 represent the spectrum least affected by the interference pattern and this spectrum should be considered as an ideal one.

Apparently, this kind of measurement and comparison of the very edges (at low α) of the spectrum for a variety of patterns is not trivial, and furthermore, the edge difference is not always distinguishable. However, a practical criterion can be used to simplify this measurement. We have demonstrated experimentally that a spectrum showing a minimized difference between the E^{04} and E_{Tauc} will always show the least interference fringe impact on the transmission spectrum. In other words, the Brewster angle is the one which should result in a spectrum having equivalent E^{04} and E_{Tauc}

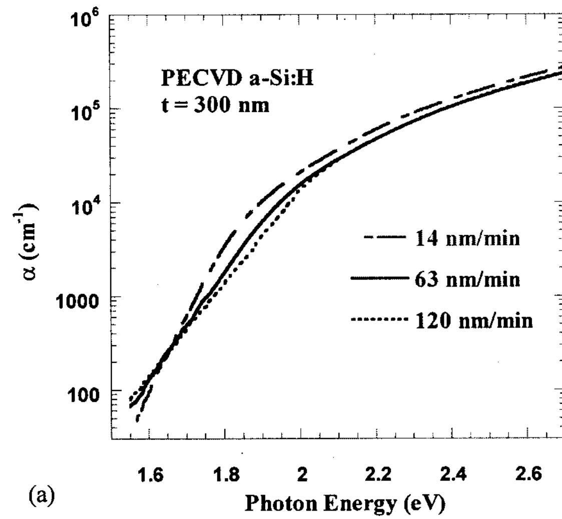

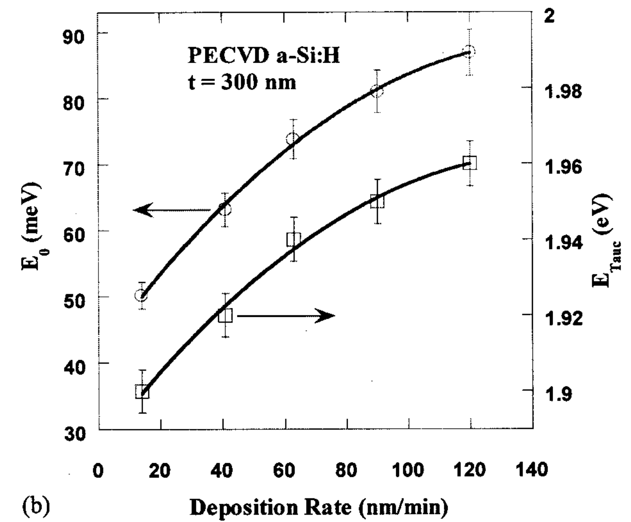

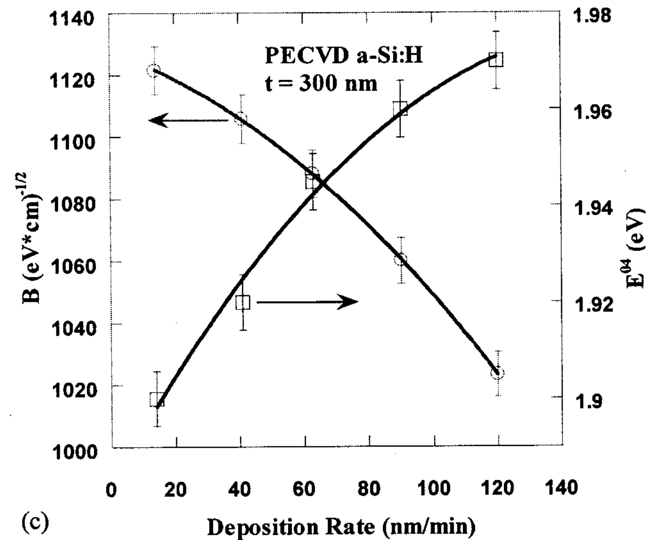

FIG. 8. (a) Absorption coefficients as a function of photon energy for a-Si:H films deposited at different rates; (b) Urbach energies (E_0) and Tauc optical band-gap (E_{Tauc}) variation as a function of a-Si:H deposition rate; (c) B values and E^{04} variations as a function of a-Si:H deposition rate

values. Although the theoretical justification for this practical method remains unclear at this time, this method will greatly simplify measurement and data processing.

The variation of the difference between the E^{04} and E_{Tauc} values with the light incident angle is shown in Fig. 7 for *a*-Si:H and *a*-SiN$_x$:H, where the $E^{04}-E_{\mathrm{Tauc}}$ values are normalized by their corresponding E^{04} (1.9 and 4.68 eV for *a*-Si:H and *a*-SiN$_x$:H, respectively) values at the Brewster angles. Since the E_{Tauc} defined by the slope at the large α is not sensitive to the interference effect, the effect of the light incident angle on E_{Tauc} is small. In contrast, since E^{04} is defined at the low absorption edge, the light incident angle exhibits a large effect on the E^{04} value, as shown in Fig. 6. Thus, the difference between E^{04} and E_{Tauc} must vary with the light incident angles.

For *a*-Si:H, the normalized $E^{04}-E_{\mathrm{Tauc}}$ value slightly increases first with the incident angle. Beyond the peak at around 50°, it starts to decrease dramatically and reaches a minimum at about 76°. Further increase of the light incident angle results in a dramatic increase of $E^{04}-E_{\mathrm{Tauc}}$. Meanwhile, for *a*-SiN$_x$:H, the difference between E^{04} and E_{Tauc} is monotomically decreasing with the light incident angle before it reaches a minimum at about 63°. Beyond the minimum point this difference starts to increase again. The data shown in Fig. 7 and the spectra shown in Figs. 4 and 5 clearly suggest that $E^{04}-E_{\mathrm{Tauc}}$ is very small (about zero) at the Brewster angle.

It should be noted in Fig. 7 that *a*-Si:H and *a*-SiN$_x$:H exhibit different trends before the curves reach their minimum. This discrepancy is due to a significant difference between the refractive indices of these two films. Specifically, *a*-Si:H has a large refractive index, and hence, exhibits a strong reflection at the interfaces due to large index differences between air (1) and *a*-Si:H (4.01) as well as between *a*-Si:H (4.01) and the quartz substrate (1.5). Meanwhile, *a*-SiN$_x$:H has a comparatively smaller refractive index and exhibits a weak reflection at the film's interfaces due to the small index differences between the film and surrounding media. Therefore, for *a*-Si:H, the interference strength is sufficient to impact the large α region, as shown in Figs. 4(a) and 5, though the impact is not significant. This will result in a small E^{04} as well as a small E_{Tauc} shown in Figs. 4 and 5. With the increase of the light incident angle, the interference impact disappears more rapidly in a large α region than in a small α region. That is the reason why a larger difference is observed with the increasing light incident angle. With the light incident angle approaching the Brewster angle, the interference impact becomes negligible in a large α region and E_{Tauc} becomes constant while E^{04} is still changing towards an ideal value (or E_{Tauc}). Thus, the $E^{04}-E_{\mathrm{Tauc}}$ difference is reduced again until it reaches a minimum. On the other hand, for *a*-SiN$_x$:H, since the interfacial reflections are not intense, the interference impact in a large α region has never been strong enough to alter the E_{Tauc} value significantly for a large $E^{04}-E_{\mathrm{Tauc}}$ difference to be observed. A monotomical decrease of the $E^{04}-E_{\mathrm{Tauc}}$ difference with the light incident angle (less than Brewster) is observed in Fig. 7. It may be concluded that the film with a smaller refractive index exhibits a more rapid $E^{04}-E_{\mathrm{Tauc}}$ difference variation as a function of the light incident angle, and vice versa.

VI. APPLICATION

The optical properties derived from the fringe-free spectrum can be used for a variety of material assessments. For instance, Fig. 8(a) illustrates the comparison of the absorption coefficients as functions of photon energy for PECVD *a*-Si:H thin films deposited at different deposition rates (d). As indicated in Fig. 8, the films deposited at different rates show different low α band tails around $10^3\ \mathrm{cm}^{-1}$ as well as different E^{04} values, while their large α shoulders are very similar. From Fig. 8, the correlation between the Urbach edge or optical band gap and the film's deposition rate can well be established. As given in Fig. 8(b), both E_0 and E_{Tauc} increasing with the *a*-Si:H deposition rate indicates an increase of the structural and thermal disorder within the film with the increase of the deposition rate. Likewise, Fig. 8(c) shows the B (slope) value and E^{04} variation as functions of the *a*-Si:H deposition rate. The decrease of the B value and increase of E^{04} with the *a*-Si:H deposition rate agree well with that indicated in Fig. 8(b). These rate dependences are consistent with the variation of other material properties, and with the associated changes of the *a*-Si:H TFT's electrical performance.[19]

VII. CONCLUSION

We have presented a practical method to obtain an interference-free transmission spectrum of hydrogenated amorphous solid thin films. Based on this resultant spectrum, reliable optical properties of the films can be obtained directly. The crucial step of this method is the choice of the right light incident angle. This convenient method is based on the minimization of the difference between E^{04} and E_{Tauc} values. The key procedures to obtain reliable optical properties can be summarized in three steps. First, collect spectra at several different light incident angles, which should be varied within the presumed correct range. Second, extract and compare all E^{04} and E_{Tauc} values for all different angles, and identify the one that yields closest E^{04} and E_{Tauc} values. Finally, deduce all the optical properties from the final spectrum that is obtained for the $E^{04}E_{\mathrm{Tauc}}\approx 0$ condition.

ACKNOWLEDGMENTS

This work was supported by AFOSR/ARPA through the Multi-disciplinary University Research Initiative (MURI) under Contract No. F49020-95-1-0524, and by the Center for Display Technology and Manufacturing at the University of Michigan.

[1] W. Fuhs, in *Amorphous and Microcrystalline Semiconductor Devices*, edited by J. Kanicki (Artech House, Norwood, MA, 1991), Vol. II.
[2] M. Vanecek, A. Abraham, O. Stoika, J. Struchlik, and J. Kocka, Phys. Status Solidi A **83**, 617 (1984).
[3] K. Pierz, B. Hilgenberg, H. Mell, and G. Weiser, J. Non-Cryst. Solids **97/98**, 63 (1987).
[4] K. Tanaka, and Y. Yamasaki, Philos. Mag. B **56**, 79 (1987).
[5] W. B. Jackson, and N. M. Amer, Phys. Rev. B **25**, 5559 (1982).

[6] G. D. Cody, B. Abeles, C. Wronski, C. R. Stephens, and B. Brooks, Sol. Cells **2**, 227 (1980).
[7] T. Li, C. Y. Chen, C. T. Malone, and J. Kanicki, Mater. Res. Soc. Symp. Proc. **424**, 43 (1996).
[8] A. R. Forouhi, and I. Bloomer, Phys. Rev. B **34**, 7018 (1986).
[9] J. Tauc, *Amorphous and Liquid Semiconductors* (Plenum, New York, 1974).
[10] E, Hecht, *Optics*, 2nd ed. (Addison-Wesley, 1989), Chap. 8.
[11] G. R. Fowles, *Introduction to Modern Optics*, 2nd ed. (Dover, New York, 1989), Chap. 2.
[12] J. D. Joannopoulos, and G. Lucovsky, Topics in Appl. Phys. **56**, 61 (1984), edited by J. D. Joannopoulos and G. Lucovsky (Springer-Verlag, New York).
[13] J. Ristein, and G. Weiser, Sol. Energy Mater. **12**, 221 (1985).
[14] Beyond these spectral regions the absorption of films becomes so significant that little energy will be left to engage interference.
[15] N. Maley and I. Szafraned, Mater. Res. Soc. Symp. Proc. **192**, 663 (1990).
[16] O. S. Heavens, *Optical Properties of Thin Solid Films* (Dover, New York, 1965), Chap. 4.
[17] $\because \tan\ \theta_B = \tan(90° - \theta_r) = 1/\tan\theta_r = n_r/n_i \therefore \tan\ \theta_r = n_i/n_r = \tan\theta'_B \Rightarrow$ Brewster condition.
[18] T. Li and J. Kanicki, J. Appl. Phys. **85**, 388 (1999).
[19] T. Li (unpublished results).